# A mathematical model of tumour angiogenesis: Growth, regression, and regrowth

Guillermo Vilanova* [1], Ignasi Colominas[1], and Hector Gomez[2]

[1] *Departamento de Métodos Matemáticos e de Representación, Grupo de Métodos Numéricos en Ingeniería – Universidade da Coruña, Campus de Elviña, 15071, A Coruña, Spain*
[2] *School of Mechanical Engineering, Purdue University, 585 Purdue Mall, West Lafayette, IN 47907, USA*

December 16, 2016



**Abstract**

Cancerous tumours have the ability to recruit new blood vessels through a process called angiogenesis. By stimulating vascular growth, tumours get connected to the circulatory system, receive nutrients, and open a way to colonise distant organs. Tumour-induced vascular networks become unstable in the absence of tumour angiogenic factors. They may undergo alternating stages of growth, regression, and regrowth. Following a phase-field methodology, we propose a model of tumour angiogenesis that reproduces the aforementioned features and highlights the importance of vascular regression and regrowth. In contrast with previous theories which focus on vessel remodelling due to the absence of flow, we model an alternative regression mechanism based on the dependency of tumour-induced vascular networks on tumour angiogenic factors. The model captures capillaries at full scale, the plastic dynamics of tumour-induced vessel networks at long time scales, and shows the key role played by filopodia during angiogenesis. The predictions of our model are in agreement with *in vivo* experiments and may prove useful for the design of antiangiogenic therapies.

**Subject areas:** Computational biology.
**Keywords:** Angiogenesis, capillary regression and regrowth, mathematical modelling.

## 1 Introduction

Angiogenesis is the growth of new capillaries from pre-existing blood vessels. The growth process is usually triggered by cells whose oxygen or nutrient requirements are not satisfied by the current vasculature and it can happen both in physiological and pathological conditions [1]. Notably, angiogenesis plays a pivotal role in tumour development because it is a necessary step for a solid tumour to grow beyond a certain size and become malignant [2].

In cancer, tumour cells proliferate abnormally quickly consuming the oxygen and nutrient released by pre-existing blood vessels. As a consequence, they generate hypoxic regions within the tumour. Hypoxic cancerous cells may release tumour angiogenic factors (TAFs) [3], such as vascular endothelial growth factor (VEGF) or basic fibroblast growth factor (bFGF) [4, 5], that unbalance the equilibrium between pro- and anti- angiogenic substances in their microenvironment. Endothelial cells (those that line the interior surface of blood vessels) are able to sense this change through their surface receptors. This activates the angiogenic response, a complex process that includes: selection of tip endothelial cells (TECs, those that will lead capillary growth); degradation of the basement membrane; sprout initiation; tip endothelial cell migration towards the hypoxic region; proliferation of the capillary stalk to elongate the vessel; formation of the lumen that allows blood flow; and anastomoses between capillaries to form loops [6]. Angiogenesis peaks with the formation of a new vascular network. The newly developed network provides cancerous cells with virtually limitless oxygen and nutrients, as well as a way to escape the primary tumour and potentially metastasise.

Tumours give rise to dense, tortuous, and defective capillary networks (see figure 1a), which are significantly different from those formed in physiological conditions [7]. Arguably, the most characteristic feature of tumour-induced capillaries is that they are TAF-dependent as suggested by experiments [8–11]. Specifically, in [10], Mancuso and coworkers performed *in vivo* experiments where newly-formed capillaries regressed after chemically inhibiting VEGF receptor signalling of endothelial cells (figure 1b). Perhaps more importantly, the experiment showed that tumour-induced capillaries regrew when VEGF receptors were made functional again (figures 1c to 1d). Due to this evidence, it is currently believed that vascular regression can also hap-

*Corresponding author: gvilanovac@udc.es

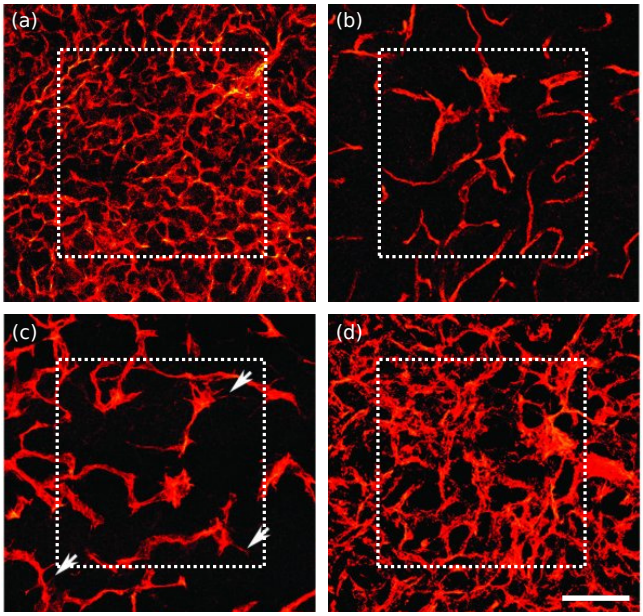


**Figure 1.** Tumour angiogenesis *in vivo*. (a) Growth of capillaries in a Rip-Tag2 tumour; (b) regressed capillaries after a 2-day inhibition of vascular endothelial growth factor receptors; (c) regrowth of first sprouts (arrows) 2 days after inhibition removal; and (d) regrown capillaries 7 days after removal. Scale bar: 115 µm (Adapted from [10]).

pen locally and spontaneously in areas which are temporarily well oxygenated. After local regression, nearby tumour cells become hypoxic again, activating back the angiogenesis cascade. Mancuso et al. also observed in their work that regressing capillaries leave (temporarily) behind the vascular membrane that enveloped them. When new capillaries regrew afterwards, these vascular membranes were used by TECs as a scaffold that facilitated their migration: By going through these empty sleeves of basement membrane, TECs avoid or at least minimise the effort of degrading the ECM. As a consequence, the authors also observed that the regrowth was faster than the normal growth. Notably, the role of detecting the basement membranes relies on filopodia. Filopodia are receptor-rich, slender cytoplasmatic protrusions that TECs extend to enhance their sensitivity, to prove their microenvironment, and to respond to it. In particular, when filopodia sense the remnants of basement membrane, TECs alter their direction towards them to use them as the path of minimum resistance in their migration.

There is an emerging view that regression and regrowth may play a significant role in the long-term dynamics of tumour angiogenesis and cancer development [12, 13]. Numerous investigations have shed light on the intricate growth of capillaries through mathematical models (see [14–16] for extensive reviews). In the literature we found different strategies to model capillaries. Some approaches use fully continuous theories that represent capillaries as averaged endothelial cell concentrations [17–21]. Although they set the basis for angiogenesis modelling, either they are fundamentally unable to capture the structure of capillaries or they only model the onset of angiogenesis. Using a different approach, several authors developed models such as [22–29] based on one-dimensional discrete theories for the description of tip endothelial cells. In these models, capillaries are defined as the trail of tip endothelial cells, capturing thus the medial line of the capillaries, but not their width. Continuing with discrete theories, another common approach is to model every endothelial cell using full-scale agent-based theories, as in [30–32]. These theories are able to define the faulty structure of capillaries, but are, in turn, computationally demanding. Lately, the phase field theory [33, 34] has been used to model angiogenesis [35–39]. This theory is based on the definition of an order parameter that typically takes two values, each one representing a "phase". The intermediate region between these two phases is a thin, smooth transition which in the limit becomes a sharp interface. The order parameter is interpreted in angiogenesis as a marker of the location of the endothelial cells, such that one phase represents the capillaries, the other the extravascular region, and the interface the capillary wall. The dynamics of the capillaries is governed by a partial differential equation that minimises an energy functional. The phase field model allows to resolve capillaries at full scale and to represent their structure. Furthermore, because it is not computationally expensive, the theory can capture the long-term dynamics of angiogenesis, or can be coupled with tumour growth models [37, 40]. We also envision phase-field theories of angiogenesis being coupled with three-dimensional fluid dynamics simulations to compute blood flow [41].

In the last years, new or augmented mathematical models of tumour-induced angiogenesis have been developed to include more biological phenomena, such as vascular adaptation, vessel remodelling, blood flow, and capillary collapse [16, 42, 43]. In these theories, neo-vessels are no longer viewed as static, but they adapt to the changes of their environment. One of the first works on this topic was pioneered by Secomb and Pries [44], in which vessels changed their radius as a function of wall shear stress, intravascular pressure, and short- and long-range metabolic stimuli. This one dimensional theory for blood flow has also been used in two and three dimensional models of angiogenesis such as [45–52], which also include phenomena such as varying vessel radii, haematocrit, non-Newtonian effects, or subcellular dynamics. The interested reader is referred to the above-mentioned reviews for further works on this topic. In these theories, capillary remodelling depends upon blood flow. However, its dependency on tumour angiogenic factor and the long-term dynamics of regression and regrowth has received little attention. In this work, we present a model for tumour angiogenesis that includes not only growth of new capillaries, but their natural regression and regrowth subject to tumour angiogenic factor availability. The model, based on the phase field theory, resolves capillaries at full scale, allowing a description of their structure. We analyse the long-term dependency of this structure upon external stimuli. Our results achieve good agreement with *in vivo* experiments and suggest that our model could be a useful tool for the design of antiangiogenic therapies, which are emerging as a promising treatment for cancer [53].

## 2 Mathematical model

Our formulation accounts for three essential ingredients of angiogenesis, namely, TAF, capillaries, and tip endothelial cells (TECs), as shown in figure 2. In our theory, TAF is interpreted as one general and potent angiogenic factor, for instance VEGF, for the wide variety and functions of TAFs makes it effectively impossible to account for everyone. We model TAF as a normalised continuous variable $f \in [0, f_{\text{HYC}}]$ representing the concentration of the factor. Capillaries are modelled using an order parameter $c \in [-1, 1]$, such that the areas where $c \geq 0$ are identified with the endothelial cells that form capillaries and those where $c < 0$ represent the extravascular tissue. Furthermore, as capillaries are enveloped by a basement membrane and occasionally by a thin cell coverage (pericytes and smooth muscle cells), we extend the definition of $c$ to include them: The extravascular tissue is compartmentalised into the capillary coverage, $-0.9 < c < 0$, and the extracellular matrix, $c < -0.9$. Finally, TECs are modelled as discrete agents which follow

chemical cues and sense nearby capillaries or empty basement membranes left by regressed capillaries.

### 2.1 Tumour angiogenic factor

TAF is produced by tumour cells when they enter a hypoxic state. Tumour cells are located at fixed points and are assumed to be hypoxic when they do not have a capillary closer than the oxygen diffusion length, $\delta_{\text{nox}}$ (figure 2). TAF diffuses from the hypoxic cells (HYCs) and throughout the tissue, decays naturally, is consumed by endothelial cells, and eventually triggers angiogenesis. Its dynamics is supposed to be governed by the reaction-diffusion equation

$$\frac{\partial f}{\partial t} = \nabla \cdot (D \nabla f) + \mathcal{P}(d)\,(f_{\text{HYC}} - f) - \mathcal{U}(c)\, f, \qquad (1)$$

where $D$ is the diffusion coefficient and $f_{\text{HYC}}$ is a constant representing the maximum tumour angiogenic factor concentration in the tissue. $\mathcal{P}$ is defined as

$$\mathcal{P}(d) = \begin{cases} P & \text{if } d < R \\ 0 & \text{if } d \geq R \end{cases}. \qquad (2)$$

Here, $P$ is the production rate, $d$ is the distance to the closest hypoxic tumour cell, and $R$ is an average cell radius. The term $\mathcal{P}(d)\,(f_{\text{HYC}} - f)$ in equation (1) limits the concentration of TAF within a hypoxic cell to $f_{\text{HYC}}$. The uptake function $\mathcal{U}$ is defined as

$$\mathcal{U}(c) = \begin{cases} U_u c & \text{if } c \geq 0 \\ -U_d c & \text{if } c < 0 \end{cases}, \qquad (3)$$

where $U_u$ is the endothelial cell uptake rate, and $U_d$ combines the TAF decay rate and the uptake rate by other cells. The uptake function acts such that deep inside the capillaries where $c = 1$ the uptake term $-\mathcal{U}(c)\, f$ of equation (1) reduces to $-U_u f$, that is, the endothelial cell uptake. On the other hand, when $c = -1$, the term reduces to $-U_d f$ which accounts for natural decay. Note that natural decay is neglected inside capillaries, as the uptake by endothelial cells is two orders of magnitude higher than natural decay, i.e., $U_u >> U_d$. In the intermediate region the uptake function creates a transition between the endothelial cell uptake and the natural decay.

### 2.2 Capillaries

The dynamics of capillaries is modelled using the phase field theory. While at tissue scales averaged descriptions of the capillaries may be enough, at the scale at which we study angiogenesis, that is cellular to tissue scale, the morphology of the new vascular networks plays an important role. For instance, the location of new sprouts alters the distribution of tumour angiogenic factor, oxygen, and hypoxic regions and the width and connections of capillaries influences blood flow. The phase field model allows to describe this morphology without tracking the evolution of the capillary walls. Following this theory, the evolution of the order parameter $c$ that represents a marker of the location of endothelial cells is such that it tends to adopt the configuration of minimum energy given by the energy functional

$$\mathcal{E}(c, f) = \int_{\Omega} \Big( \Psi_s(c) + \Psi_c(c, f) \Big) d\mathbf{x}, \qquad (4)$$

where $\Psi_s$ and $\Psi_c$ are the so-called surface free energy and chemical free energy, respectively. The surface free energy is defined as

$$\Psi_s(c) = \frac{1}{2}\lambda^2 |\nabla c|^2, \qquad (5)$$

where $\lambda$ is a constant proportional to the width of the capillary wall. This term accounts for the required energy to create and maintain the capillary wall. The chemical free energy, defined as

$$\Psi_c(c, f) = \frac{1}{4}(c+1)^2(c-1)^2 + \frac{1}{2}\alpha\gamma(f)(c+1)^2(2-c), \qquad (6)$$

is a double-well, non-convex function with two local minima (as shown on the top row of figure 3) where $\alpha$ is a parameter and $\gamma(f)$ is a tilting function. Each local minimum represents a phase. The first one is at $c = 1$, where the concentration of endothelial cells is maximum, while the other is at $c = -1$, where there are no endothelial cells; that is, the extravascular tissue. Between them there is a local maximum such that the energy contribution $\Psi_c$ leads to the separation of the phases. Furthermore, the second term on the right-hand side of equation (6), by means of the function $\gamma(f)$, tilts the double-well favouring one phase over the other. This term captures the following proliferative to apoptotic phenotype switch. Endothelial cell receptors stimulated by TAF activate molecular pathways that change the cell phenotype either to a migratory (TECs, modelled separately) or to a proliferative one. In the absence of stimuli, endothelial cells lining immature, tumour-induced capillaries become apoptotic, which eventually leads to vascular regression [13]. Hence, we define $\gamma(f)$ as

$$\gamma(f) = \exp\left[-\exp(\beta(f - f_{\text{act}}))\right] - \exp(-1), \qquad (7)$$

where $\beta$ is a constant. As shown in figure 3, this function tilts the double well in such a way that capillary growth (proliferative phenotypes) is favoured when $f > f_{\text{act}}$ and capillary regression (apoptotic phenotypes) is promoted otherwise. In equation (6), the parameter $\alpha$ is set to guarantee the existence of two local minima in $\Psi_c$ for all $\gamma$.

The key idea to successfully model this phenotype switch is to make use of non-conserved phase-field dynamics rather than previously used conserved models [36]. In the latter, the energy structure of the phase-field would be broken down by the incorporation of a reactive term. This new approach, however, allows a seamless integration of proliferation and apoptosis of endothelial cells in the energy functional. Thus, our phase-field equation is

$$\frac{\partial c}{\partial t} = -M \frac{\delta \mathcal{E}}{\delta c} \qquad (8)$$

where $M$ is the mobility, a positive time-scale parameter, and

$$\frac{\delta \mathcal{E}}{\delta c} = -\lambda^2 \Delta c + \mu(c, f) \qquad (9)$$

is the variational derivative of the energy $\mathcal{E}$. In equation (9),

$$\mu(c, f) = \frac{1}{2}\left(c^2 - 1\right)\left(c - 3\alpha\gamma(f)\right) \qquad (10)$$

is the derivative of $\Psi_c$ with respect to the order parameter. Finally, we end the derivation of the phase field equation gathering equations (8) and (9), which leads to the following reaction-diffusion partial differential equation:

$$\frac{\partial c}{\partial t} = M\left(\lambda^2 \Delta c - \mu(c, f)\right). \qquad (11)$$

The reader is referred to [54–57] for detailed descriptions of this kind of phase-field models often used in dendritic solidification, but also in biological problems [58].

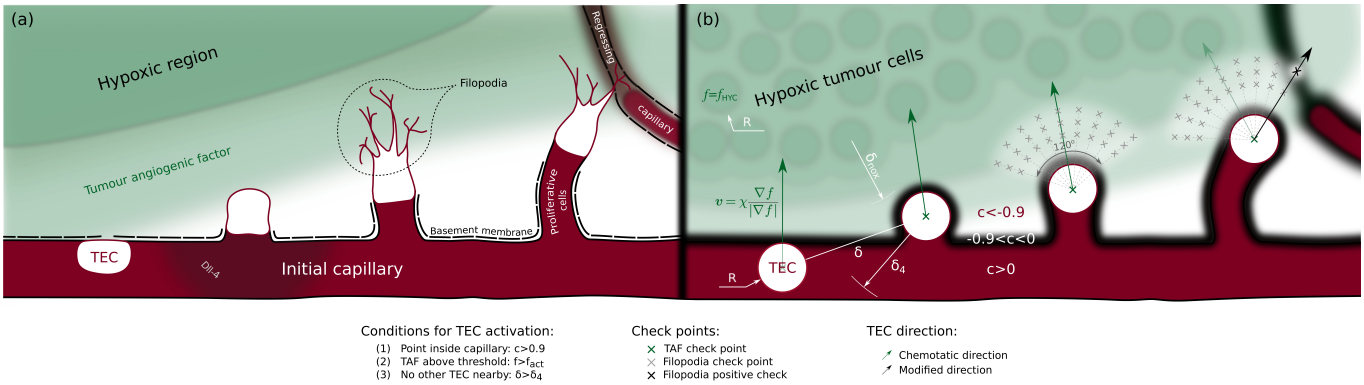


**Figure 2.** Conceptualisation of tip endothelial cells. (a) Tumour angiogenic factor (TAF) activates tip endothelial cells (TECs) that extend filopodia to survey their environment. (b) In the model, discrete circular agents are activated and migrate following TAF gradients. Each agent evaluates conditions at filopodia check points. A positive check ($c > -0.9$) alters the (otherwise chemotactic) migration direction.

## 2.3 Tip endothelial cells

When capillaries receive TAF signals, some privileged cells (TECs) acquire a migratory phenotype and lead the growth of new sprouts [59]. This phenotype was not included in equations (7), (10), and (11). When an endothelial cell becomes a TEC, it expresses Delta-like ligand 4 (Dll-4). Dll-4 binds to Notch receptors of nearby endothelial cells preventing them from becoming also TECs [60, 61]. This mechanism is known as *lateral inhibition*. TECs migrate following cues that guide the new capillaries towards nutrient-demanding cells. These cues may be, for example, chemical or mechanical. TECs are especially sensitive to such cues because they extend highly-dynamic, receptor-rich protrusions called filopodia [62, 63] towards the angiogenic stimuli (see figure 2a). Furthermore, as filopodia probe the cell's microenvironment, they may detect nearby endothelial cells. In this event, the TEC anastomoses with the identified endothelial cell forming a loop between the growing sprout and the detected capillary. Note that this mechanism increases the vascular network connectivity. Perhaps more surprisingly, filopodia may even sense basement membranes left behind by regressed capillaries and use them to improve their migratory capacity (see [64] and the supporting information therein for examples of *in vitro* experiments). The fact that no other cell will become migratory in the vicinity of a TEC through the lateral inhibition mechanism, makes tip endothelial cells ideally suited for a discrete description. A prime example is the work by Bentley *et al.* [65, 66] which predicts TEC selection combined with migration and fusion using a cell-scale agent based model.

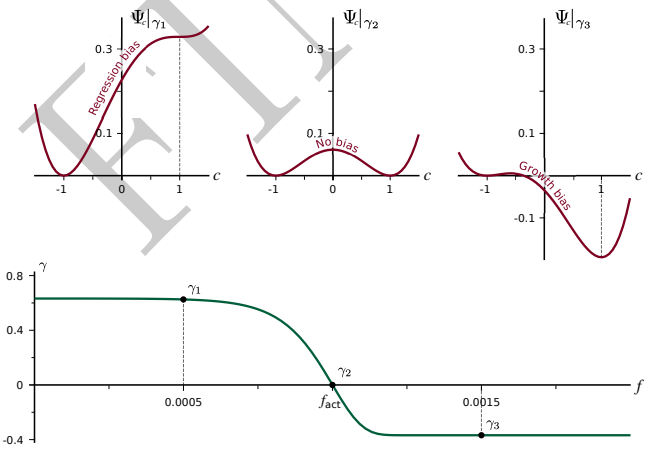


**Figure 3.** Chemical energy and tilting function. The chemical free energy $\Psi_c$ (in red), is a double-well potential tilted by the tumour angiogenic factor value through the function $\gamma(f)$ (in green). Low values of tumour angiogenic factor bias the evolution of $c$ towards regression (top-left graph), while high values of tumour angiogenic factor promote growth (top-right graph).

Thus, TECs are discrete agents in our formulation, as shown in figure 2b. They are modelled using ideas from the literature [35], but further extended to include filopodia, to detect nearby capillaries, and to migrate not only following chemotactic cues (figure 2b, green arrows) but also using the empty sleeves of basement membrane left in the extracellular matrix (figure 2b, black arrow) by regressed capillaries. Following [35], we use discrete agents that are characterised by their centre and their radius $R$. TEC activation, that is, the phenotype switch from quiescent or proliferative to migratory, is performed according to the following deterministic rules: A point of the domain is the centre of a new TEC if

1. it is inside a capillary ($c > c_{\text{act}}$), to guarantee that it is an endothelial cell;
2. the tumour angiogenic factor is greater than a threshold ($f > f_{\text{act}}$), to assure that the stimulus is potent; and
3. there is no other TEC in the vicinity (distance to every TEC greater than $\delta_4$), to account for the Delta-Notch selection.

Activated cells, unless they detect a nearby basement membrane or a capillary, migrate through the extracellular matrix following chemotactic cues with a velocity proportional to the TAF gradient, given by

$$\mathbf{v} = \chi \frac{\nabla f}{|\nabla f|}, \tag{12}$$

where $\chi$ is the chemotactic constant and $|\cdot|$ denotes the Euclidean norm.

In our model, TECs also develop filopodia, which we model as a set of check points that mimic their high concentration of receptors (figure 2b, grey crosses). Because tumour angiogenic factors polarise tip cells such that they spread filopodia towards their front [59], we evenly place the check points into an annular sector of angle $\theta = 2\pi/3$ centred around the chemotactic direction, as shown in figure 2b. The internal and external radius of the annular sector are set to $\ell_{\text{int}} = 2R$ and $\ell_{\text{ext}} = 4R$, respectively, which is within the range of filopodia length [62]. Filopodia do not develop immediately after TEC activation, thus, in the model, the check points are not tested until the sprout has been initiated, that is, until the TEC has migrated a diameter from its activation point and it is outside its parent vessel. A positive check (figure 2b, black cross), defined as $c > -0.9$, means that the TEC has detected a basement

**Table 1.** Parameters of the model in dimensionless units.

| Parameter | Description | In-text reference | Value |
|---|---|---|---|
| $D$ | Tumour angiogenic factor diffusion coefficient | Equation (1) | 350.0 |
| $f_{\text{HYC}}$ | Maximum tumour angiogenic factor concentration in the tissue | Equation (1) | 1.0 |
| $P$ | Tumour angiogenic factor production by HYCs | Equation (2) | 350.0 |
| $R$ | Average cell radius | Equation (2) | 4.0 |
| $U_u$ | Tumour angiogenic factor endothelial cell uptake | Equation (3) | 21.875 |
| $U_d$ | Tumour angiogenic factor natural decay | Equation (3) | 0.35 |
| $\lambda$ | Interface width | Equation (5) | 1.0 |
| $\alpha$ | Phenotype switch | Equation (6) | 0.525 |
| $\beta$ | Phenotype switch | Equation (7) | $10^4$ |
| $M$ | Mobility | Equation (8) | 0.0875 |
| $\chi$ | Chemotatic constant of tip endothelial cells | Equation (12) | 25.48 |
| $c_{\text{act}}$ | Condition for TEC activation | Condition 1 | 0.9 |
| $f_{\text{act}}$ | Condition for TEC activation | Condition 2 | 0.001 |
| $\delta_4$ | Dll-4 radius of action | Condition 3 | 32.0 |
| $\delta_{\text{nox}}$ | Nutrient and oxygen diffusion length | | 20.0 |

membrane or a capillary through filopodia. Under this circumstance, the (chemotactic) direction of migration is altered towards the check point. Furthermore, the velocity magnitude is doubled when tip cells move using the vascular membrane scaffold to account for the easier migration through the already-degraded extracellular matrix. In the event of several positive checks, the check point where the value of $c$ is higher is selected.

There are two ways by which a TEC can be deactivated, that is, the endothelial cell looses its migratory phenotype. The first one occurs when the TEC anastomoses with another TEC or capillary. Anastomosis is modelled in a similar way to filopodia: TECs test the value of $c$ in an $2\pi/3$-radians arc with radius $R$ centred around the direction of migration. If any of these values is greater that 0.9, that is, the TEC is already touching the capillary, then there is an anastomosis event and the TEC gets deactivated. The second deactivating circumstance happens when the stimulus ceases (failure to meet condition 2). In both cases the discrete agent is removed.

Finally, to close the model, we need to couple the discrete agents and the continuous variables. The connection between these two parts of the model is that both the TECs and the continuous variable $c$ describe endothelial cells. Thus, we include TECs in the phase-field variable using a straightforward approach: $c$ is updated to $c = 1$ in those regions of the computational domain occupied by TECs. Further elaborated strategies could be used to conciliate the discrete agents with the phase-field theory at the expense of a greater complexity. In addition, other discrete models for TECs that also operate at the cellular scale such as [66] could be easily coupled with this model using the proposed approach.

## 2.4 Numerical methods

Our theory is composed by two continuum variables and a set of discrete agents. Thus, we develop numerical methods for the partial differential equations, for the discrete agents, and for coupling both of them. First, we derive the weak form of the continuous partial differential equations (1) and (11) and we discretise them in space and time using the Galerkin method and the generalised-$\alpha$ method [67, 68], respectively (see text T1 in the electronic supplementary material). Isogeometric Analysis [69, 70] permits us to use globally smooth functions on the domain and a means of accurately solve the equations. Additionally, we implement a time-step correction algorithm similar to those in [71–73]. Then, we develop an algorithm that handles TEC activation, filopodia probing, migration, and deactivation. Note that the migration of TECs is meshless, meaning that it is independent of the spatial discretisation of the continuum variables. This fact hinders the coupling between the discrete agents and the continuum variables, which we perform by updating the value of the order parameter $c$ at the locations of tip endothelial cells every time step using the concept of templates presented in [36]. Thus, each time step $t_n$ before solving the continuous partial differential equations, we replace the phase field $c$ with

$$\widetilde{c}(\mathbf{x}, t_n) = \begin{cases} g_c^j(\mathbf{x}) & \text{if } \mathbf{x} \in \Omega_{\text{TEC}}^j, \\ c(\mathbf{x}, t_n) & \text{otherwise.} \end{cases} \tag{13}$$

for all $j = 1, \ldots, N_{\text{TEC}}$, where $N_{\text{TEC}}$ is the number of active TECs, $\Omega_{\text{TEC}}^j$ is the domain of the $j$-th TEC, and the template function $g_c^j$ is a multidimensional generalisation of an exact one-dimensional solution to the phase-field equation on an infinite domain (see details in [36]). Note that the implemented adaptive time-step scheme could yield a large time step, which in turn, could create a gap between capillaries and TECs. Hence, the continuous/discrete coupling limits the maximum time step size so that each time step a TEC is moved a maximum of 10% of its radius.

The parameter values in dimensionless units used in the computations are summarised in table 1. The physical quantities of these parameters may be retrieved by using the length and time scales $L_0 = 1.25\,\mu\text{m}$ and $T_0 = 5460\,\text{s}$, respectively. Some of them are taken from *in vivo* observations, while others have been used in previous models of tumour angiogenesis.

The diffusion coefficient of the tumour angiogenic factor, following [35, 74], has been set to $D = 8.64 \times 10^{-9}\,\text{cm}^2\,\text{s}^{-1}$. In the model, the radius of the tip endothelial cells is $5\,\mu\text{m}$, which is within its measured 5 to 10 µm range [75]. We define the endothelial cell uptake as $U_u = D/R^2 = 14.42\,\text{h}^{-1}$ so that the tumour angiogenic factor cannot penetrate inside a capillary farther than the radius of a tip endothelial cell. The value of the natural decay rate, $U_d = 0.230\,\text{h}^{-1}$, is set so that its half-life is 3 h, an averaged value between tumour angiogenic factors [76, 77]. $P$ controls the production of TAF within a hypoxic cell. In the model, it acts as a penalty parameter that needs to be sufficiently large, without compromising the stability of the numerical scheme; thus, we have set its value to 350. As shown in the supplementary material, the solution has proven to be fairly insensitive to variations of this parameter. The tumour angiogenic factor condition for TEC activation $f_{\text{act}}$ is set to 0.001 so that for $f_{\text{HYC}} = 1$ hypoxic cells located farther than 200 µm away from a capillary can activate TECs within the timescale of angiogenesis (see text T1 in the electronic supplementary

material). Furthermore, we have set $\delta_4$ to $8R$ so that TECs impede the activation of other TECs in their neighbourhood.

The migration of TECs is controlled by the chemotactic constant $\chi$ which is set to $0.504\,\mathrm{mm\,d^{-1}}$, which is within the range of velocities observed in the mouse cornea micropocket angiogenesis assays [78]. On the other hand, proliferation and apoptosis of stalk cells is controlled by the phase field equation, in particular by the velocity of the interface. For a straight interface it can be proven [79] that this velocity is $V = 3M\lambda\alpha\gamma(f)$. Here, $\alpha$ and $\lambda$, are computational parameters which do not directly relate with physical measures. The reader can find in the electronic supplementary material a parametric study of these quantities. As shown in [79], the condition $\alpha\gamma(f) < 1/6$ is necessary to guarantee the existence of two minima in the energy functional and recalling that $\lambda$ is a fixed length scale that defines the capillary wall thickness, we can assume that the proliferation/apoptosis velocity is controlled by the mobility $M$. Because the diffusion of TAF is much faster than cell dynamics, we have set the ratio between the diffusion coefficient and the mobility to 4000. In addition, the definition of $\gamma$ is such that the velocity of capillary regression through apoptosis is 5/3 times slower than its proliferation, to maintain the integrity of growing capillaries. $\beta$ is a computational parameter that has been set to $10^4$ to produce a smooth transition in $\gamma$ around $f_{\mathrm{act}}$. Finally, under physiological conditions, every cell is at a maximum of 100 to 200 µm from a blood vessel. Because of the faulty structure of tumour-induced capillaries and the high nutrient uptake of cancer cells, we have reduced this distance to $\delta_{\mathrm{nox}} = 25\,\mu\mathrm{m}$. In this respect, the model could be improved by adding nutrient and flow compartments so that $\delta_{\mathrm{nox}}$ would not need to be estimated.

## 3 Results

We open this section with a simple simulation whose aim is to give insight and study the proposed mathematical model. The study is continued with an analysis of the parameters that control filopodia extension. Then, we show how the theory is able to capture the growth patterns in configurations that resemble *in vivo* experimental setups, in particular in a two-dimensional simulation of the mouse corneal micropocket angiogenesis assay. Finally, we present the full potential of this new theory in a simulation that replicates the experiment shown in figure 1.

### 3.1 Basic features of the model

In order to study how the model works, we perform a simple simulation on a square domain (figure 4 and video V1 in the electronic supplementary material). The simulation is performed on a $375\,\mu\mathrm{m} \times 375\,\mu\mathrm{m}$ square domain using a mesh composed by $256^2$ quadratic elements (see figure 4a); a configuration that has already proven to accurately capture the phase-field interface [36, 80]. The boundary conditions for this and every other simulation hereafter are zero-flux conditions. We consider this setup simple because, contrary to the following simulations in this paper, it only has an initial straight capillary and one HYC located close to it – approximately 60 µm away. Furthermore, for the sake of simplicity, we have set $f_{\mathrm{HYC}}$ to 0.1 to reduce the potential number of new capillaries.

Figures 4b to 4j show the time evolution of this simulation by means of zoomed snapshots. The simulation starts with TAF being produced at the HYC which diffuses throughout the domain. The first activation of a TEC (dotted, red circumferences in figure 4) occurs when enough TAF infiltrates the initial capillary, that is, when the amount of TAF is greater than $f_{\mathrm{act}}$ (green lines in figure 4) inside the capillary. Several time steps afterwards, two other TECs get activated on both sides of the first one. Note that all TECs are separated from each other as dictated by the lateral inhibition mechanism. As shown in figure 4b, the three TECs initially migrate following the chemotactic direction, marked with green arrows. Figure 4c reveals, however, that the chemotactic direction may be altered. There, the filopodia of the rightmost TEC detect the presence of a capillary located on its left-hand side. Consequently, the chemotactic direction is overridden and, even though the green arrow points to the top-right corner, the TEC moves towards the detected capillary, anastomoses with it, and gets immediately deactivated. This event highlights that anastomosis is driven by filopodia contact sensing rather than through chemotaxis in our model, which is in agreement with recent *in vivo* observations [63]. Meanwhile, the two other TECs, that have already promoted the deactivation of the HYC, continue their migration through the extracellular matrix still following chemotactic cues. Proliferative cells keep widening and elongating the capillaries. And, as shown in figure 4d, the growth process evolves unaltered until all TAF gets consumed.

At this point, in the absence of TAF, the endothelial cells of the tumour-induced vasculature, which are highly TAF-dependent, change their phenotype to an apoptotic one and regression starts. Figures 4e to 4g show how this process, although slower than the initial growth (note the time steps on the captions and its duration in the video), promotes the gradual disappearance of the capillaries. The vascular basement membrane that was enveloping the capillaries, however, remains after the capillaries have regressed forming the already mentioned empty sleeves, through which future TECs can migrate easily[1]. And, indeed, after the HYC gets activated again the new TECs that orchestrate the regrowth, aided by their filopodia, use these remnants of basement membrane to direct the formation of new capillaries (figures 4h to 4j). As shown in figure 4j, the regrowth and the growth pattern are not equal, even in this simple setup. The source of this difference is that TECs migrate faster through the empty sleeves than through the extracellular matrix, thus, their velocities are higher with respect to TAF consumption. In particular, in the regrowth process shown in that figure a new TEC gets activated soon after the anastomosis event between the rightmost TEC and the middle capillary, creating a new sprout that grows towards the top-right corner.

### 3.2 Parametric study of filopodia

In the previous example we observe how filopodia play a pivotal role in creating anastomoses between capillaries. The parameters that define filopodia probing, that is $\theta$, $\ell_{\mathrm{int}}$, and $\ell_{\mathrm{ext}}$ were estimated from observations [64]. Note that the parameter $\ell_{\mathrm{int}}$ measures the minimum distance at which filopodia start to sense. Its value has been set to a minimum $2R$ so that TECs does not sense themselves. There is no biological reason to increase this parameter, either. Therefore, we perform here an study of the value of the other parameters. As shown in figure 5a, for this study we make use of a more realistic, although still academic configuration of the computational domain. Initially, we place two capillaries along opposite edges of the square domain and an aggregate of hypoxic cells at its centre. These HYCs represent hypoxic regions of a 112.5 µm-diameter tumour. The size of the domain and mesh used for this simulation are the same as in the previous example (see figure 4a).

First we present in figure 5b two snapshots of the evolution of the vascular network for $\theta = 2\pi/3$ and $\ell_{\mathrm{ext}} = 4R$, that

[1] Given enough time, the basement membranes would eventually regress.

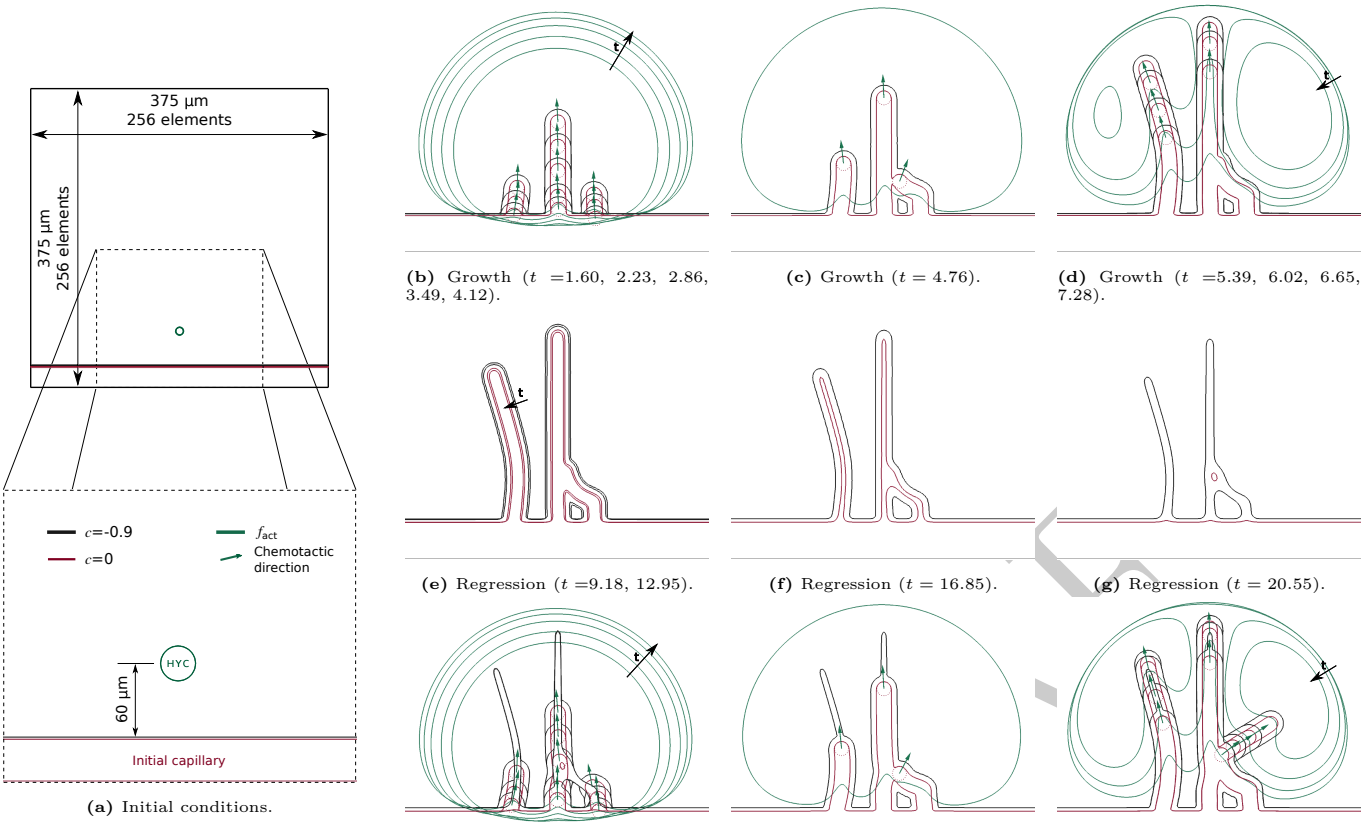


**(a)** Initial conditions.

**(b)** Growth ($t$ =1.60, 2.23, 2.86, 3.49, 4.12).

**(c)** Growth ($t$ = 4.76).

**(d)** Growth ($t$ =5.39, 6.02, 6.65, 7.28).

**(e)** Regression ($t$ =9.18, 12.95).

**(f)** Regression ($t$ = 16.85).

**(g)** Regression ($t$ = 20.55).

**(h)** Regrowth ($t$ = 22.45, 23.06, 23.72, 24.33, 24.95).

**(i)** Regrowth ($t$ = 25.60).

**(j)** Regrowth ($t$ = 26.23, 26.85, 27.48, 28.36).

**Figure 4.** Basic features of the model. Simulation of the mathematical model in a simplistic setup (a) that shows the process of growth (b-d), regression (e-g), and regrowth (h-j).

is, the estimated values. In the first snapshot we observe that the longest capillaries, those created first, grow parallel to each other separated by a distance close to $\delta_4$. However, as more capillaries grow behind, the distance between TECs and capillaries falls within the extension range of filopodia, which triggers the creation of anastomoses. The network starts to form loops until a lattice-like pattern that spans and oxygenates the tumour gets generated at time $t = 30$. In the remaining sub-figures we show the vascular patterns at that time generated under the same initial conditions and parameters, except for one. In figures 5c and 5d we have altered the maximum extension of the filopodia twice and thrice, respectively. As the detection range of TECs has been increased, tip cells detect nearby capillaries easily. Indeed, the scope of filopodia is now greater or equal to $\delta_4$, meaning that TECs sense other capillaries as soon as they initiate the formation of a new sprout. The resulting networks create an hourglass-like shape with the thinnest part over the tumour. This shape is more pronounced in figure 5d, where a higher value of $\ell_{\text{ext}}$ favours the creation of aberrant capillary clusters. In the simulation shown in figure 5e we have decreased the spread angle of filopodia $\theta$ to $5\pi/12$ and in figure 5f we have increased it to $11\pi/12$. In the former case the highly reduced detection by filopodia promotes a vascular network of capillaries than run parallel and only get occasionally connected by short vessels. In the latter, we observe a small number of top-to-bottom capillaries from which many short sprouts emerge. These sprouts get rapidly connected (in many instances even with its parent capillary) due to the large value of $\theta$, creating capillary masses and saccular regions.

In this parametric study we have shown that the vascular patterns for the altered parameters are more defective either by forming clusters of capillaries or by creating parallel, poorly interconnected ones. Note, however, that in experimental observations the direction and extent of filopodia is not constant, but varies widely. In the absence of data we have estimated these parameters as constants for the sake of simplicity, although a more complicated stochastic model could be easily incorporated.

### 3.3 Vascular growth

As a first illustration of the capabilities of our model in an experimental-like setup, we show in figure 6 a computation in a configuration that resembles the mouse cornea micropocket angiogenesis assay [81]. The cornea is an avascular tissue surrounded by a region called limbus formed by capillaries. Tumour cells in the cornea may promote the creation of new capillaries from the limbus. Thus, in our simulation, the entire system is initially avascular (figure 6a), except for a circular capillary (red) that mimics the limbal vessels. We include a cluster of hypoxic tumour cells that release a generic tumour angiogenic factor (green) that triggers angiogenesis. Figure 6b shows a snapshot of the growing capillaries that are pervading the cornea and forming a new vessel network. As this network grows, endothelial cells consume angiogenic factor and tumour cells that are close to capillaries become normoxic and stop releasing TAF. Capillaries grow led by tip endothelial cells. TECs follow gradients of tumour angiogenic factor (triangle-labelled discrete agent of the inset), unless they sense nearby capillaries through filopodia (star-labelled agent of the same inset) and anastomose with them. The pattern obtained in this numerical simulation immediately after capillary growth has ceased (figure 6c) is similar to those observed *in vivo* [81–83] and *in silico* [24, 26, 84].

We performed a quantification of the neovasculature over time (figure 6d). The vasculature starts as a tree-like net-

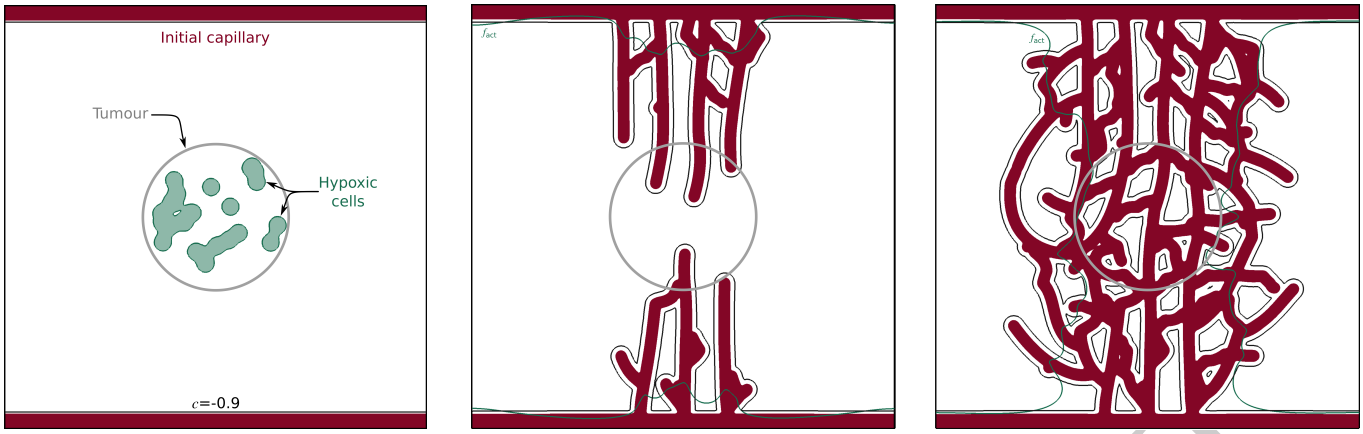


**(a)** Initial conditions.

**(b)** Two snapshots (right; $t = 20, 30$, respectively) of the formation of a a vascular network using the estimated parameters $\theta = 2\pi/3$ and $\ell_{\text{ext}} = 4R$.

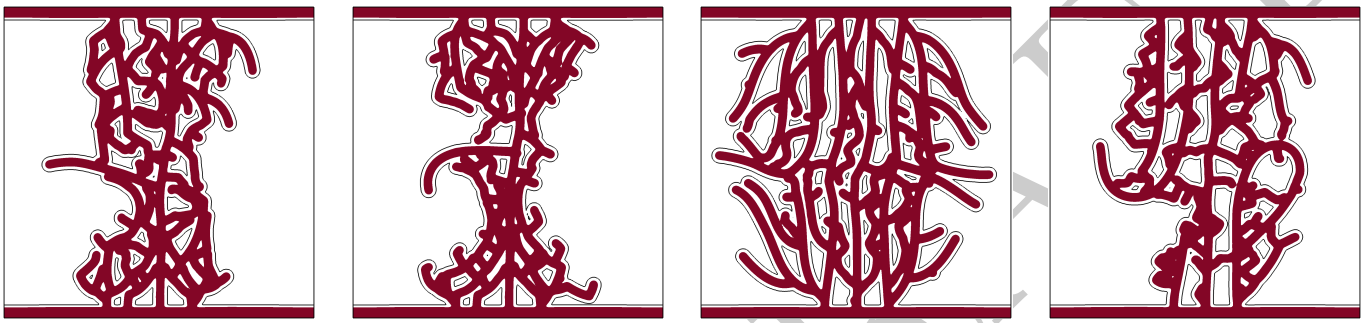

**(c)** Vascular pattern at time $t = 30$ for $\ell_{\text{ext}} = 8R$.

**(d)** Vascular pattern at time $t = 30$ for $\ell_{\text{ext}} = 12R$.

**(e)** Vascular pattern at time $t = 30$ for $\theta = 5\pi/12$.

**(f)** Vascular pattern at time $t = 30$ for $\theta = 11\pi/12$.

**Figure 5.** Parametric study of filopodia. Tumour angiogenesis is induced by the TAF released by a hypoxic cells aggregated in a tumour-like circular region (a). The simulations show the comparison of the vascular patterns generated with the estimated parameters of the model (b) and variations of these parameters (b-e). In the first case the resulting pattern is more connected and regular at time $t = 30$ than in the remaining cases.

work (no loops) driven by an increasing number of TECs that create new branches and bifurcations. However, as their filopodia detect nearby capillaries, the number of anastomosis events grows rapidly. Consequently, the tree-like network gradually evolves to a mesh-like one with loops that facilitate blood flow. By the end of the simulation approximately 30 anastomoses have shaped the vasculature into a highly-interconnected network with more than 20 loops. Note that by the end of the simulation more than 50% of the loops involve four capillary branches or more (> 4-loops). These long-range connections favour the oxygenation of tumour cells. The pace at which the vasculature penetrates the cornea (measured as the distance from the limbus to the innermost TEC using the shortest path) is linear, as reported in [82, 83]. We also measured the maximum and average capillary length (distance between bifurcations) and observed that anastomoses reduce the maximum length compared to the penetration distance and maintain the average length almost constant.

With the aim of evaluating the role of filopodia, we repeated the same simulation disabling the extension of filopodia in each tip cell. Video V2 presents the side-by-side vascular network evolution of both simulations and figure 6e shows a comparison of the resulting medial lines or skeleton of the final patterns. Visual observation reveals two marked differences between them. The first one is that in the absence of functional filopodia, chemotactically-driven TECs chiefly migrate in the same direction creating almost parallel capillaries. The second one is that the number of anastomoses, represented as grey dots in the figure, is drastically reduced from one simulation to the other. These facts are supported by the quantitation of the last simulation shown in figure 6f. There, we observe that, although the number of TECs created during angiogenesis is almost the same, the number of bifurcations is reduced by a factor of two. Not only that, but the majority of these bifurcations are a consequence of the initiation of angiogenesis from the limbus and not due to anastomoses. The absence of filopodia prevents TECs from sensing nearby vessels and the only anastomosis event is the result of a tip cell that runs close to a capillary. As a consequence, the new vasculature presents a single loop and is mainly formed by dead-end capillaries that prevent blood flow. Note also that the duration of both simulations is equal and that both networks penetrate approximately the same distance into the cornea.

### 3.4 Regression and regrowth

The result in figure 6 illustrates the capabilities of the model to predict vascular growth patterns, but a major goal of this work was to develop a model that naturally leads to regression and regrowth. We study this phenomenon motivated by the *in vivo* experiment shown in figure 1. To replicate the experiment, we need first to simulate the growth process. To this end, we chose as our computational domain the area enclosed by the dotted lines in figure 1. In the simulation, the system is initially avascular, except for a capillary placed on the boundary which serves as a precursor to the neo-vasculature (figure 7a). Randomly distributed hypoxic cells (that resemble the Rip-Tag2 tumour in the experiment) release angiogenic factor that activates tip endothelial cells. Initially, capillaries grow inwards, forming a new vasculature (figure 7b). Then, the vasculature regresses due to the absence of tumour angiogenic factor (figure 7c) and the system enters a transient behaviour with local regressions and regrowths (see video V3 in the electronic supplementary material) similar to those observed in experiments. Figures 7d to 7h show snapshots of different patterns that highlight the

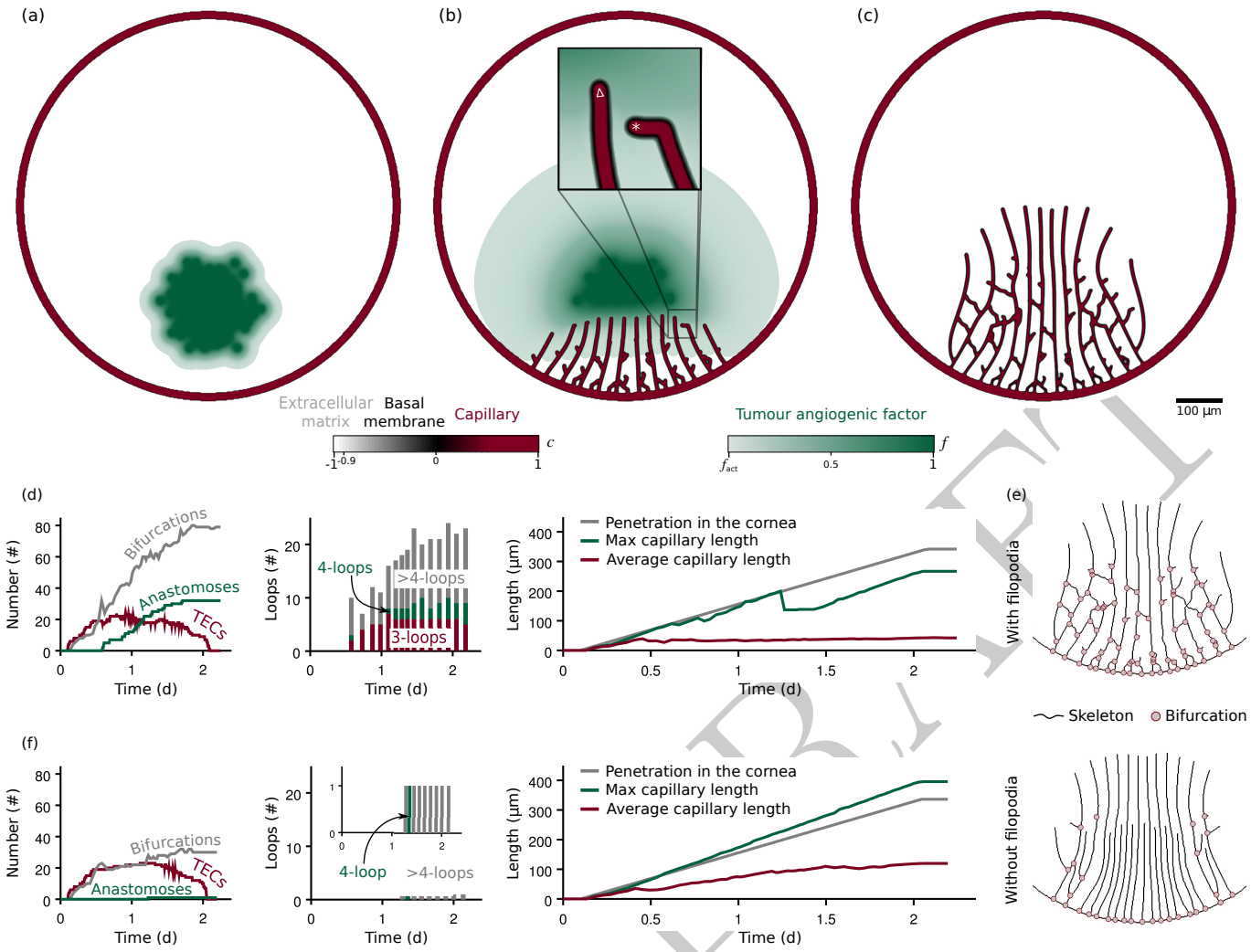


**Figure 6.** Corneal neovascularisation. (a) Circular initial capillary (red) and cluster of tumour cells that release tumour angiogenic factor (green). (b) Tip endothelial cells (TECs) lead the growth of the new capillaries. (c) Vascular pattern after growth. (d) Neovasculature quantification. (e) Skeletons of the final patterns of the simulations with and without filopodia extension. (f) Quantification of the simulation without filopodia.

dynamism and adaptation of the vasculature when regression and regrowth are considered. Note that in figure 7h the initial capillary has completely regressed. We assume that this configuration is analogous to the starting point of the experiment (figure 1a).

The experimental procedure of Mancuso et al. is continued by chemically inhibiting the VEGF receptors of endothelial cells, so that capillaries are unable to detect the presence of TAF and eventually regress (figure 1b). The receptors are kept blocked for 7 days and the capillaries regrow afterwards (figures 1c to 1d). Our simulation proceeds along the same lines. We model the receptor inhibition by blocking the activation of new tip endothelial cells. Those that were active will eventually get deactivated in the absence of tumour angiogenic factor. During the inhibition, most capillaries regress, as shown in figures 7i to 7l. Note that regressed capillaries leave behind a trail (grey colours representing low values of $c$ in figure 7) which we identify with the basement membrane. If the treatment were prolonged, all the capillaries and basement membranes will eventually disappear. However, as in the experiment, we remove the inhibition after approximately 7 days (figure 7m) and the regrowth process starts (figures 7n to 7p). The high availability of TAF due to the treatment promotes an almost instant activation of TECs after its removal.

Visual inspection shows that the *in vivo* experiment and the numerical simulation compare well. In both cases the network is composed of tortuous, highly interconnected vessels that oxygenate the tissue unevenly. Also, as the new vasculature is particularly dependent on tumour angiogenic factor, the inhibition acts successfully, leaving in both cases few, barely functional capillaries in the region. The dependency on tumour angiogenic factor also implies that the vasculature recovers rapidly after the treatment, a finding that may be useful in the design of antiangiogenic therapies. Adding to the visual inspection, we performed a quantitative comparison between the simulation and the experiment. Figure 8 shows the vascular density of the former in grey and of the latter (data taken from [10]) in red. Vascular density suffers a drastic drop due to the inhibition. Then, the regrowth process starts and the vascular density eventually recovers its original value. After the regrowth, our model predicts mild oscillations of the vascular density due to spontaneous local regressions and regrowths. To some extent, this can also be inferred in the experiment, but there is insufficient data to be conclusive. In addition, in order to pose the mathematical model we had to make several assumptions. One of the strongest ones is that we neglect the proliferation and death of cancerous cells and assume fixed hypoxic regions, as the time scale of angiogenesis is smaller than that of tumour growth. In this experiment in particular, we presume that the tumour is not aggressive and remains constant and occupying the whole domain throughout the duration simulation. This assumption hinders the quantitative comparison with assays. In summary, although precise agreement with *in vivo* experiments is a daunting task, the simulation captures the

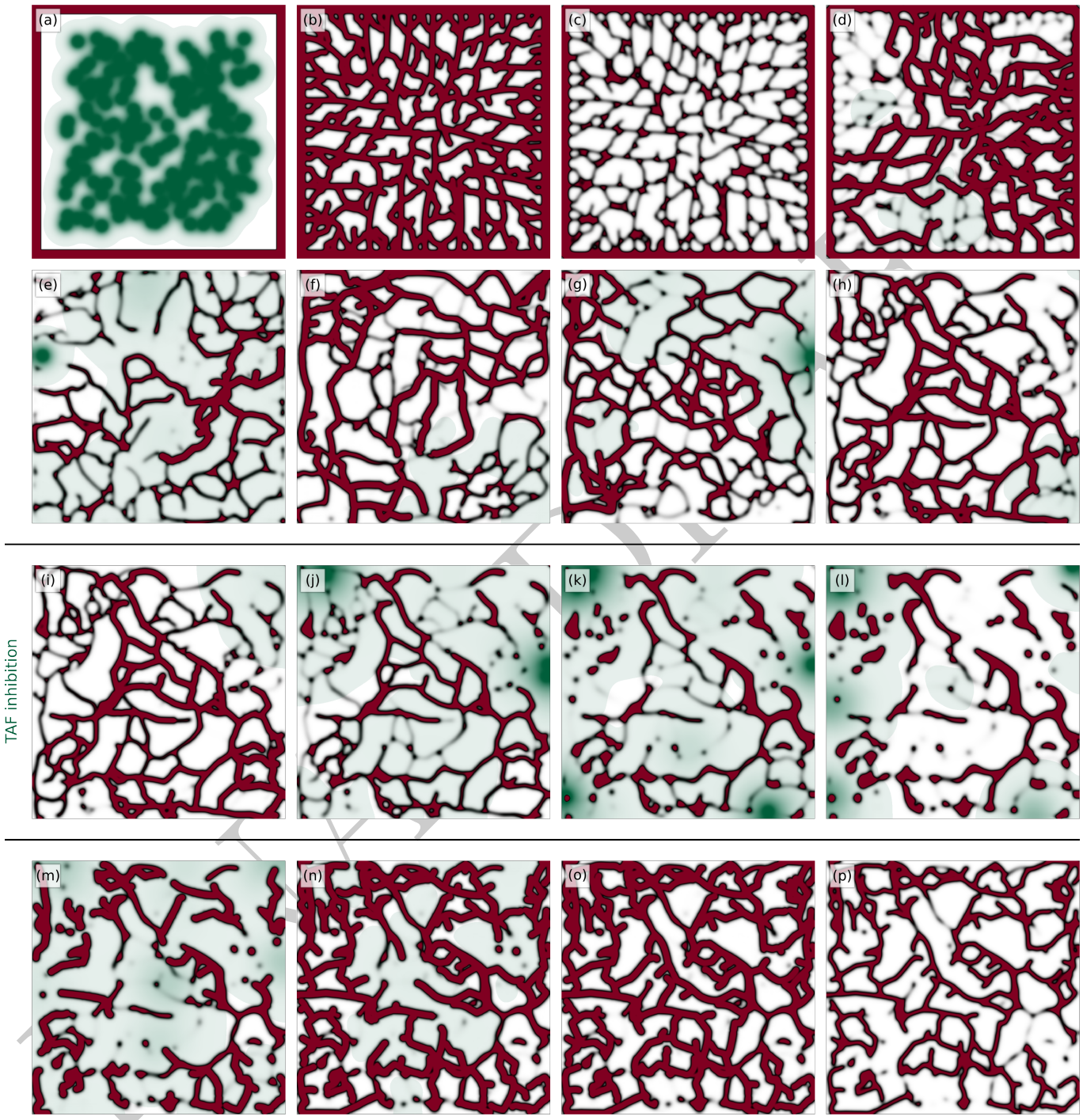


**Figure 7.** Tumour angiogenesis simulation: growth, regression, and regrowth. (a-h) Snapshot of the growth phase of angiogenesis. (i-l) The chemical inhibition of tumour angiogenic factor receptors promotes capillary regression during 7 days. (m-p) When the inhibition is removed, new tip endothelial cells get activated and start the regrowth process. The vasculature recovers its original density 7 days after the inhibition removal. This simulation replicates the experiment of figure 1 and both are compared in figure 8. Colour legend in figure 6.

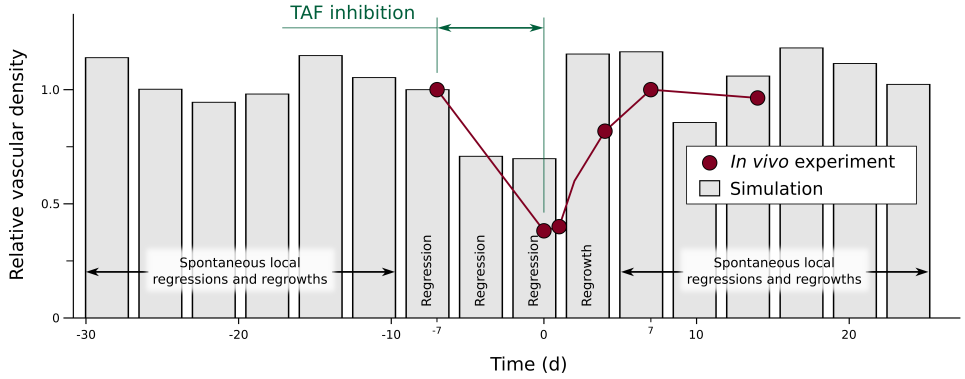


**Figure 8.** Evolution of the relative vascular density (current vascular density over a reference vascular density). Both the experiment (red, figure 1) and the simulation (grey, figure 7) show regression promoted by TAF inhibition, followed by regrowth after the inhibition is over.

trend of the experiment.

## 4 Conclusions

In this work, we have presented a new model for tumour-induced angiogenesis growth, regression, and regrowth. The model is based in a non-conservative phase-field theory which, opposite to previous models that include vessel remodelling, allows to resolve capillaries at full scale and to simulate long-term dynamics of angiogenesis. Existing models consider vessel regression and remodelling mainly based on one-dimensional theories of blood flow [44, 45]. Here, we model an alternative regression mechanism which emanates from the fact that tumour-induced capillaries are TAF dependent. In addition, we have included a discrete conceptualisation of filopodia that endows tip endothelial cells with the ability to sense their microenvironment.

Even assuming a fixed tumour and neglecting blood flow, our model predicts the plasticity and dynamic evolution of capillaries at long time spans. In particular, the simulations are in agreement with *in vivo* experiments and capture capillary regression induced by TAF inhibition and their subsequent regrowth after inhibition removal. Our simulations reinforced the view that filopodia-based sensing plays a major role in anastomosis and loop formation and that chemotaxis itself is not enough to create connected networks that favour blood flow and oxygenation. Furthermore, filopodia have proven to facilitate regrowth, as they enhance TEC exploration of the least resistant path for migration, which is formed by the left-behind basement membranes. In this respect the model could be augmented by explicitly considering extracellular matrix degradation during migration and making TEC velocity a function of this new variable. Also, the directional switch of TEC migration between the chemotactic and vessel detection by filopodia could be improved by incorporating a smooth transition based on experimental data.

In conclusion, our model reinforces the view that tumours need to be analysed as a complex system which interacts dynamically with its microenvironment. In this context, our study highlights the importance of regression and regrowth of tumour vasculature. The proposed model may be a useful tool not only to predict capillary growth patterns, but also for the design of antiangiogenic therapies, which are currently considered the fourth pillar of cancer treatment after surgery, chemotherapy, and radiation.

## Authors' contributions

G.V. and H.G. conceived and designed the research. G.V. run the simulations. G.V., H.G., and I.C. analysed the data. G.V., H.G., and I.C. participated in the preparation and editing of the manuscript.

## Acknowledgements

The authors gratefully acknowledge the support from the European Research Council, Xunta de Galicia, ConsellerÄšía de Cultura, Educación e Ordenación Universitaria, Ministerio de Economía y Competitividad, and FEDER.

## Funding statement

GV and HG were partially supported by the European Research Council (contract #307201), Xunta de Galicia, and by Ministerio de Economía y Competitividad (contract #DPI-2013-44406-R, cofinanced with FEDER funds). IC was partially supported by Consellería de Cultura, Educación e Ordenación Universitaria of the Xunta de Galicia (grant #GRC2014/039).

## References

[1] Carmeliet P. Angiogenesis in life, disease and medicine. Nature (London). 2005;438(7070):932–936.

[2] Folkman J. Tumor angiogenesis: Therapeutic implications. N Engl J Med. 1971;285(21):1182–1186.

[3] Hanahan D, Weinberg RA. Hallmarks of cancer: The next generation. Cell. 2011;144(5):646–674.

[4] Tahtis K, Bicknell R. Tumour Angiogenesis. In: Knowles M, Selby P, editors. Introduction to the Cellular and Molecular Biology of Cancer. Oxford University Press Inc.; 2005. p. 289–302.

[5] Weis SM, Cheresh DA. Tumor angiogenesis: molecular pathways and therapeutic targets. Nat Med. 2011;17(11):1359–1370.

[6] Carmeliet P, Jain RK. Molecular mechanisms and clinical applications of angiogenesis. Nature (London). 2011;473(7347):298–307.

[7] Carmeliet P, Jain RK. Angiogenesis in cancer and other diseases. Nature (London). 2000;407(6801):249–257.

[8] Inai T, Mancuso MR, Hashizume H, Baffert F, Haskell A, Baluk P, et al. Inhibition of Vascular Endothelial Growth Factor (VEGF) Signaling in Cancer Causes Loss of Endothelial Fenestrations, Regression of Tumor Vessels, and Appearance of Basement Membrane Ghosts. Am J Pathol. 2004;165(1):35–52.

[9] Baffert F, Le T, Sennino B, Thurston G, Kuo CJ, Hu-Lowe D, et al. Cellular changes in normal blood capillaries undergoing regression after inhibition of VEGF signaling. Am J Physiol Heart Circ Physiol. 2006;290(2):H547–H559.

[10] Mancuso MR, Davis R, Norberg SM, O'Brien S, Sennino B, Nakahara T, et al. Rapid vascular regrowth in tumors after reversal of VEGF inhibition. J Clin Invest. 2006;116(10):2610–2621.

[11] Falcon BL, Barr S, Gokhale PC, Chou J, Fogarty J, Depeille P, et al. Reduced VEGF Production, Angiogenesis, and Vascular Regrowth Contribute to the Antitumor Properties of Dual mTORC1/mTORC2 Inhibitors. Cancer Res. 2011;71(5):1573–1583.

[12] Goel S, Duda DG, Xu L, Munn LL, Boucher Y, Fukumura D, et al. Normalization of the Vasculature for Treatment of Cancer and Other Diseases. Physiol Rev. 2011;91(3):1071–1121.

[13] Potente M, Gerhardt H, Carmeliet P. Basic and Therapeutic Aspects of Angiogenesis. Cell. 2011;146(6):873–887.

[14] Mantzaris NV, Webb S, Othmer HG. Mathematical modeling of tumor-induced angiogenesis. J Math Biol. 2004;49(2):111–187.

[15] Lowengrub JS, Frieboes HB, Jin F, Chuang YL, Li X, Macklin P, et al. Nonlinear modelling of cancer: Bridging the gap between cells and tumours. Nonlinearity. 2010;23(1):R1–R9.

[16] Scianna M, Bell CG, Preziosi L. A review of mathematical models for the formation of vascular networks. J Theor Biol. 2013;333:174–209.

[17] Byrne HM, Chaplain MAJ. Mathematical models for tumour angiogenesis: Numerical simulations and nonlinear wave solutions. Bull Math Biol. 1995;57(3):461–486.

[18] Orme ME, Chaplain MAJ. Two-dimensional models of tumour angiogenesis and anti-angiogenesis strategies. Math Med Biol. 1997;14(3):189–205.

[19] Peterson JW, Carey GF, Knezevic DJ, Murray BT. Adaptive finite element methodology for tumour angiogenesis modelling. Int J Numer Method Biomed Eng. 2007;69(6):1212–1238.

[20] Valero C, Javierre E, García-Aznar JM, Gómez-Benito MJ. Numerical modelling of the angiogenesis process in wound contraction. Biomech Model Mechanobiol. 2013;12(2):349–360.

[21] Connor AJ, Nowak RP, Lorenzon E, Thomas M, Herting F, Hoert S, et al. An integrated approach to quantitative modelling in angiogenesis research. J R Soc Interface. 2015;12(110).

[22] Anderson ARA, Chaplain MAJ. Continuous and discrete mathematical models of tumor-induced angiogenesis. Bull Math Biol. 1998;60(5):857–899.

[23] Chaplain MAJ. Mathematical modelling of angiogenesis. J Neurooncol. 2000;50(1-2):37–51.

[24] Tong S, Yuan F. Numerical simulations of angiogenesis in the cornea. Microvasc Res. 2001;61(1):14–27.

[25] Sun S, Wheeler MF, Obeyesekere M, Patrick CW. A deterministic model of growth factor-induced angiogenesis. Bull Math Biol. 2005;67(2):313–337.

[26] Harrington HA, Maier M, Naidoo L, Whitaker N, Kevrekidis PG. A hybrid model for tumor-induced angiogenesis in the cornea in the presence of inhibitors. Math Comp Model. 2007;46(3-4):513–524.

[27] Milde F, Bergdorf M, Koumoutsakos P. A hybrid model for three-dimensional simulations of sprouting angiogenesis. Biophys J. 2008;95(7):3146–3160.

[28] Das A, Lauffenburger D, Asada H, Kamm RD. A hybrid continuum-discrete modelling approach to predict and control angiogenesis: Analysis of combinatorial growth factor and matrix effects on vessel-sprouting morphology. Philos Trans R Soc London, Ser A. 2010;368(1921):2937–2960.

[29] Watson MG, McDougall SR, Chaplain MAJ, Devlin AH, Mitchell CA. Dynamics of angiogenesis during murine retinal development: a coupled in vivo and in silico study. J R Soc Interface. 2012;9(74):2351–2364.

[30] Alarcón T, Byrne HM, Maini PK. A multiple scale model for tumor growth. Multiscale Model Simul. 2005;3(2):440–475.

[31] Bazmara H, Soltani M, Sefidgar M, Bazargan M, Mousavi Naeenian M, Rahmim A. The Vital Role of Blood Flow-Induced Proliferation and Migration in Capillary Network Formation in a Multiscale Model of Angiogenesis. PLoS ONE. 2015;10(6):1–31.

[32] Shirinifard A, Gens JS, Zaitlen BL, Popławski NJ, Swat M, Glazier JA. 3D Multi-Cell Simulation of Tumor Growth and Angiogenesis. PLoS ONE. 2009;4(10):e7190.

[33] Emmerich H. Advances of and by phase-field modelling in condensed-matter physics. Advances in Physics. 2008;57(1):1–87.

[34] Gomez H, van der Zee KG. Computational phase-field modeling. In: Encyclopedia of Computational Mechanics. John Wiley & Sons, Ltd.; In press. .

[35] Travasso RDM, Corvera Poiré E, Castro M, Rodríguez-Manzaneque JC, Hernández-Machado A. Tumor angiogenesis and vascular patterning: A mathematical model. PLoS One. 2011;6(5):e19989.

[36] Vilanova G, Colominas I, Gomez H. Capillary networks in tumor angiogenesis: From discrete endothelial cells to phase-field averaged descriptions via isogeometric analysis. Int J Numer Method Biomed Eng. 2013;29(10):1015–1137.

[37] Lima EABF, Oden JT, Almeida RC. A hybrid ten-species phase-field model of tumor growth. Math Models Methods Appl Sci. 2014;24(13):2569–2599.

[38] Santos-Oliveira P, Correia A, Rodrigues T, Ribeiro-Rodrigues TM, Matafome P, Rodríguez-Manzaneque JC, et al. The Force at the Tip - Modelling Tension and Proliferation in Sprouting Angiogenesis. PLoS Comput Biol. 2015;11(8):e1004436.

[39] Giverso C, Ciarletta P. Tumour angiogenesis as a chemo-mechanical surface instability. Sci Rep. 2016;6:22610.

[40] Xu J, Vilanova G, Gomez H. Full-scale, three-dimensional simulation of early-stage tumor growth: The onset of malignancy. Comput Methods Appl Mech Eng. 2016;p. In press.

[41] Bernabeu MO, Jones ML, Nielsen JH, Krüger T, Nash RW, Groen D, et al. Computer simulations reveal complex distribution of haemodynamic forces in a mouse retina model of angiogenesis. J R Soc Interface. 2014;11(99).

[42] Logsdon EA, Finley SD, Popel AS, Mac Gabhann F. A systems biology view of blood vessel growth and remodelling. J Cell Mol Med. 2014;18(8):1491–1508.

[43] Rieger H, Welter M. Integrative models of vascular remodeling during tumor growth. Wiley Interdiscip Rev Syst Biol Med. 2015;7(3):113–129.

[44] Pries AR, Secomb TW, Gaehtgens P. Structural adaptation and stability of microvascular networks: theory and simulations. American Journal of Physiology - Heart and Circulatory Physiology. 1998;275(2):H349–H360.

[45] Perfahl H, Byrne HM, Chen T, Estrella V, Alarcón T, Lapin A, et al. Multiscale Modelling of Vascular Tumour Growth in 3D: The Roles of Domain Size and Boundary Conditions. PLoS ONE. 2011;6(4):e14790.

[46] Owen MR, Alarcón T, Maini PK, Byrne HM. Angiogenesis and vascular remodelling in normal and cancerous tissues. J Math Biol. 2009;58(4-5):689–721.

[47] Curtis LT, Wu M, Lowengrub J, Decuzzi P, Frieboes HB. Computational Modeling of Tumor Response to Drug Release from Vasculature-Bound Nanoparticles. PLoS ONE. 2015;10(12):1–17.

[48] Wu M, Frieboes HB, McDougall SR, Chaplain MAJ, Cristini V, Lowengrub J. The effect of interstitial pressure on tumor growth: Coupling with the blood and lymphatic vascular systems. J Theor Biol. 2013;320:131–151.

[49] Macklin P, McDougall S, Anderson ARA, Chaplain MAJ, Cristini V, Lowengrub JS. Multiscale modelling and nonlinear simulation of vascular tumour growth. J Math Biol. 2009;58(4-5):765–798.

[50] Secomb TW, Alberding JP, Hsu R, Dewhirst MW, Pries AR. Angiogenesis: An Adaptive Dynamic Biological Patterning Problem. PLoS Comput Biol. 2013;9(3):e1002983.

[51] Welter M, Rieger H. Physical determinants of vascular network remodeling during tumor growth. Eur Phys J E Soft Matter. 2010;33(2):149–163.

[52] Welter M, Rieger H. Interstitial Fluid Flow and Drug Delivery in Vascularized Tumors: A Computational Model. PLoS ONE. 2013;8(8):e70395.

[53] Maxwell PH, Ashcroft M. Antiangiogenic Cancer Therapy. Br J Cancer. 2009;100(9):1515.

[54] Kobayashi R. Modeling and numerical simulations of dendritic crystal growth. Phys D. 1993;63(3-4):410–423.

[55] Provatas N, Goldenfeld N, Dantzig J. Efficient Computation of Dendritic Microstructures Using Adaptive Mesh Refinement. Phys Rev Lett. 1998;80:3308–3311.

[56] Karma A, Rappel WJ. Quantitative phase-field modeling of dendritic growth in two and three dimensions. Phys Rev E. 1998;57:4323–4349.

[57] Kim YT, Provatas N, Goldenfeld N, Dantzig J. Universal dynamics of phase-field models for dendritic growth. Phys Rev E. 1999;59:R2546–R2549.

[58] Ziebert F, Swaminathan S, Aranson IS. Model for self-polarization and motility of keratocyte fragments. J R Soc Interface. 2012;9(70):1084–1092.

[59] De Smet F, Segura I, De Bock K, Hohensinner PJ, Carmeliet P. Mechanisms of vessel branching: filopodia on endothelial tip cells lead the way. Arterioscler Thromb Vasc Biol. 2009;29(5):639–649.

[60] Hellström M, Phng LK, Hofmann JJ, Wallgard E, Coultas L, Lindblom P, et al. Dll4 signalling through Notch1 regulates formation of tip cells during angiogenesis. Nature (London). 2007;445(7129):776–780.

[61] Thurston G, Kitajewski J. VEGF and Delta-Notch: interacting signalling pathways in tumour angiogenesis. Br J Cancer. 2008;99(8):1204–1209.

[62] Gerhardt H, Golding M, Fruttiger M, Ruhrberg C, Lundkvist A, Abramsson A, et al. VEGF guides angiogenic sprouting utilizing endothelial tip cell filopodia. J Cell Biol. 2003;161(6):1163–1177.

[63] Phng LK, Stanchi F, Gerhardt H. Filopodia are dispensable for endothelial tip cell guidance. Development. 2013;140(19):4031–4040.

[64] Murakami T, Suzuma K, Takagi H, Kita M, Ohashi H, Watanabe D, et al. Time-lapse imaging of vitreoretinal angiogenesis originating from both quiescent and mature vessels in a novel ex vivo system. Invest Ophthalmol Vis Sci. 2006;47(12):5529–5536.

[65] Bentley K, Gerhardt H, Bates PA. Agent-based simulation of notch-mediated tip cell selection in angiogenic sprout initialisation. J Theor Biol. 2008;250(1):25 – 36.

[66] Bentley K, Mariggi G, Gerhardt H, Bates PA. Tipping the balance: Robustness of tip cell selection, migration and fusion in angiogenesis. PLoS Comput Biol. 2009;5(10):e1000549.

[67] Chung J, Hulbert GM. A time integration algorithm for structural dynamics with improved numerical dissipation: The generalized-$\alpha$ method. J Appl Mech. 1993;60:371–375.

[68] Jansen KE, Whiting CH, Hulbert GM. A generalized-$\alpha$ method for integrating the filtered Navier-Stokes equations with a stabilized finite element method. Comput Methods Appl Mech Eng. 2000;190(3-4):305 – 319.

[69] Hughes TJR, Cottrell JA, Bazilevs Y. Isogeometric analysis: CAD, finite elements, NURBS, exact geometry and mesh refinement. Comput Methods Appl Mech Eng. 2005;194(39-41):4135–4195.

[70] Cottrell JA, Hughes TJR, Bazilevs Y. Isogeometric analysis: Toward integration of CAD and FEA. Wiley, editor. Wiley; 2009.

[71] Gomez H, Calo VM, Bazilevs Y, Hughes TJR. Isogeometric analysis of the Cahn-Hilliard phase-field model. Comput Methods Appl Mech Eng. 2008;197(49-50):4333–4352.

[72] Gomez H, Hughes TJR. Provably Unconditionally Stable, Second-order Time-accurate, Mixed Variational Methods for Phase-field Models. J Comput Phys. 2011;230:5310–5327.

[73] Gomez H, Cueto-Felgueroso L, Juanes R. Three-dimensional simulation of unstable gravity-driven infiltration of water into a porous medium. J Comput Phys. 2013;238:217–239.

[74] Schugart RC, Friedman A, Zhao R, Sen CK. Wound angiogenesis as a function of tissue oxygen tension: A mathematical model. Proc Natl Acad Sci USA. 2008;105(7):2628–2633.

[75] Gebb S, Stevens T. On lung endothelial cell heterogeneity. Microvasc Res. 2004;68(1):1 – 12.

[76] Beenken A, Mohammadi M. The FGF family: biology, pathophysiology and therapy. Nat Rev Drug Discovery. 2009;8(3):235–253.

[77] Kleinheinz J, Jung S, Wermker K, Fischer C, Joos U. Release kinetics of VEGF165 from a collagen matrix and structural matrix changes in a circulation model. Head Face Med. 2010;6(1):17.

[78] Brem H, Folkman J. Inhibition of tumor angiogenesis mediated by cartilage. J Exp Med. 1975;141(2):427–439.

[79] Kobayashi R. A numerical approach to three-dimensional dendritic solidification. Exper Math. 1994;3(1):59–81.

[80] Vilanova G, Colominas I, Gomez H. Coupling of discrete random walks and continuous modeling for three-dimensional tumor-induced angiogenesis. Comput Mech. 2014;53(3):449–464.

[81] Rogers MS, Birsner AE, D'Amato RJ. The mouse cornea micropocket angiogenesis assay. Nat Protoc. 2007;2(10):2545–2550.

[82] Kenyon BM, Voest EE, Chen CC, Flynn E, Folkman J, D'Amato RJ. A model of angiogenesis in the mouse cornea. Invest Ophthalmol Vis Sci. 1996;37(8):1625–1632.

[83] Tong S, Yuan F. Dose response of angiogenesis to basic fibroblast growth factor in rat corneal pocket assay: I. Experimental characterizations. Microvasc Res. 2008;75(1):10–15.

[84] Tong S, Yuan F. Dose response of angiogenesis to basic fibroblast growth factor in rat corneal pocket assay: II. Numerical simulations. Microvasc Res. 2008;75(1):16–24.